

The eclipsing X-ray pulsar X-7 in M33

G. Dubus^{1,2}, P. A. Charles¹, K. S. Long³, P. J. Hakala^{4,5}, E. Kuulkers¹

¹ *University of Oxford, Dept. of Astrophysics, Keble Road, Oxford OX13RH, UK*

² *DARC, UPR 176 du CNRS, Observatoire de Paris Meudon, 5 place Janssen, 92195 Meudon, France*

³ *Space Telescope Science Institute, 3700 San Martin Dr., Baltimore MD 21218, US*

⁴ *Mullard Space Science Laboratory, University College London, Holmbury St. Mary, Dorking, Surrey RH56NT, UK*

⁵ *Observatory and Astrophysics Lab., University of Helsinki, PO Box 14, FIN-00014, Finland*

May 1997

ABSTRACT

Using our extensive *ROSAT* X-ray observations of M33, we confirm a 3.45 day eclipse period for the *Einstein* source X-7 (Larson & Schulman 1997) and discover evidence for a 0.31-s pulse period. The orbital period, pulse period and observed X-ray luminosity are remarkably similar to SMC X-1. We therefore suggest M33 X-7 is a neutron star high mass X-ray binary with a 15-40 M_{\odot} O/B companion and a binary separation of 25-33 R_{\odot} if the companion is almost filling its Roche lobe.

Key words: Galaxies:individual:M33 - Local Group - X-rays:stars - binaries:eclipsing

1 INTRODUCTION

M33 is an Sd spiral galaxy in the Local Group, which at ~ 800 kpc (van den Bergh 1991), is slightly more distant than M31. At an inclination of $i \sim 56^{\circ}$, the disk of M33 is accessible to observation without a large amount of absorption. The first X-ray studies of M33 made with the *Einstein* Observatory Imaging Proportional Counter (Long et al. 1981) and High Resolution Imager (Market & Rallis 1983; Trinchieri, Fabbiano & Peres 1988), resulted in the detection of 13 sources brighter than 10^{38} ergs⁻¹, one of which, X-7, was flagged as variable. As a result of their luminosities the X-ray sources in M33 are thought mostly to be supernova remnants or X-ray binaries, and X-7 clearly falls into the latter category. Peres et al. (1989) and later, Schulman et al. (1993; 1994) discovered eclipse episodes in X-7 and proposed a period of 1.78 days. This strongly suggests that X-7 is a High Mass X-ray Binary (HMXB). A recent reanalysis of archival *Einstein*, *ROSAT* and *ASCA* observations of X-7 by Larson and Schulman (1997) argues in favour of a 3.45 day period.

Here we discuss a considerably larger set of *ROSAT* observations of X-7 which extend over a time base of 6 years. We use these observations to confirm the 3.45 day period and report the discovery of a 0.31 s pulse period, which allow us to establish the X-ray source as a pulsating neutron star. We have used this dataset previously to discuss the temporal variability of the nuclear source X-8 (Dubus et al. 1997) (hereafter paper I). A more general discussion of all of the sources will be the topic of a future publication.

2 OBSERVATIONS

Multiple observations using either the *ROSAT* High Resolution Imager (HRI) or Position Sensitive Proportional Counter (PSPC) were carried out between 1991 and 1997 (see Trümper (1984) for instrumental details). Most of these were centered on the optical nucleus of M33 at α 1^h33^m50^s.4, δ 30°39'36" (J2000). With a luminosity of $\approx 10^{38}$ erg/s (Long et al. 1996), X-7 is easily detected in all cases. The different observations are presented in table 1. The total exposure time is 233-ks of HRI (PSPC: 50-ks) nucleus pointed observations and about 92-ks of off-centered HRI data. From the long set of HRI observations pointed at the nucleus of M33, we get a best position for X-7 of α (J2000) 1^h33^m34^s.2 and δ 30°32'08".7, with an error of 5" to 10". This is based on deriving a correction for the *ROSAT* X-ray position of the nucleus by using the accurately known optical position (de Vaucouleurs & Leach 1981).

The barycentre-corrected photon arrival times were extracted from a 1' region centered on the best position for X-7. Background counts were also extracted from a 2' radius disk centered on α 1^h33^m20^s.7 and δ 30°31'51".3 (J2000), close to X-7 and at roughly the same angle from the axis. This choice was dictated by the presence of another source close enough to X-7 that a standard background annulus would have been unreliable. Depending on the analysis method, we used the data both in arrival time format and in spacecraft orbital averages. For the latter, we group together good time intervals within 3-ks of each other (\approx orbital time within which M33 is in the field of view) and correct for background and vignetting as described in David et al. (1996). After corrections, the mean HRI count rates

arXiv:astro-ph/9810050v1 3 Oct 1998

Table 1. *ROSAT* observations of M33 X-7

Obs.	Offset (')	Dates	Duration (ks)
<i>rp23a</i>	8	1991 29–30 Jul	29.1
<i>rp23b</i>	8	1992 10 Aug	5.0
<i>rp23c</i>	8	1993 7–9 Jan	16.3
<i>rh20a</i>	7	1992 8–12 Jan	19.1
<i>rh20b</i>	7	1992 1–3 Aug	15.8
<i>rh86</i>	12	1994 1–11 Aug	16.4
<i>rh87</i>	8	1994 27 Jul – 7 Aug	30.5
<i>rh88</i>	6	1994 27 Jul – 7 Aug	24.5
<i>rh89</i>	8	1994 6–8 Aug	20.3
<i>rh60a</i>	8	1994 10–11 Aug	8.0
<i>rh46</i>	8	1995 15–15 Jan	24.6
<i>rh60b</i>	8	1995 10–16 Jul	40.9
<i>rh11n</i>	8	1996 18 Jan – 8 Feb	46.4
<i>rh11a</i>	8	1996 17–27 Jul	44.6
<i>rh03</i>	8	1997 10–14 Jan	33.9

The first three observations were made by the PSPC while the others were carried out with the HRI. Offset is the angle between X-7 and the pointing center (the nucleus of M33 in most cases). The abbreviations used correspond to the last digits of the actual sequence number.

were about 11 counts ks^{-1} (PSPC, 39 counts ks^{-1}) for X-7 and about 3.5 counts ks^{-1} (PSPC, 1 count ks^{-1}) for the background. Deadtime corrections are negligible at such low count rates.

3 ANALYSIS AND RESULTS

The analysis methods are similar to the ones applied to the nuclear source M33 X-8 described in paper I. We searched for power at frequencies between 10^{-3} and 10 Hz using a modified Fourier spectrum (see Appendix A). On corrected mean orbital fluxes, we looked for periodicities using a Lomb–Scargle normalised periodogram.

3.1 The 3.45 day eclipse period

All of the observations of X-7 which included an eclipse feature were flagged as variable with better than 99.9% confidence. We then removed the data taken during the eclipse times and found no evidence for variability, i.e., out of eclipse the source appears to be steady. We modeled the folded lightcurve from X-7 as a constant flux + linear ingress and egress + an eclipse interval with zero flux. Minimization of the five parameters (period P , mid-phase of the eclipse ϕ_{mid} , eclipse duration $\Delta\phi_{\text{eclipse}}$, ingress duration $\Delta\phi_{\text{ingress}}$, egress duration $\Delta\phi_{\text{egress}}$) led to the following best fit ($\phi=0$ corresponds to JD 2448628.5) :

$$\begin{aligned}
 P &= 298.38 \pm 0.02 \text{ ks} \\
 \phi_{\text{mid}} &= 0.88 \pm 0.02 & \Delta\phi_{\text{eclipse}} &= 0.20 \pm 0.03 \\
 \Delta\phi_{\text{ingress}} &= 0.10 \pm 0.05 & \Delta\phi_{\text{egress}} &= 0.01 \pm 0.01
 \end{aligned}$$

The errors are estimated from all the minima found with $\chi^2_{\nu} \approx 1$ using different minimization routines, initial values and number of free parameters. The period of 3.45 days is in agreement with that found by Larson et al. (1997). The values for P , ϕ_{mid} and $\Delta\phi_{\text{eclipse}}$ are quite robust and accurately fitted. $\Delta\phi_{\text{egress}}$ was always close to 0 (symetric profiles led to a reduced $\chi^2_{\nu} \approx 2$) while $\Delta\phi_{\text{ingress}}$ was always >0 . Using P , ϕ_{mid} and the associated errors,

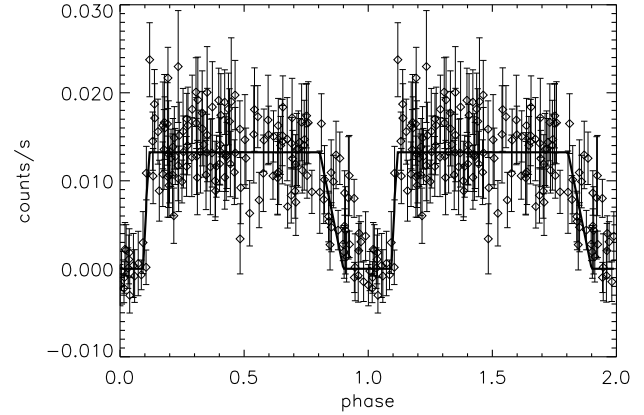


Figure 1. Folded lightcurve of X-7 over the best period of 3.45d (two cycles are represented). Each point represents an orbital flux average. The continuous line is the best fit model. Phase 0 corresponds to the mid-eclipse time derived in the text.

we derive the following ephemeris for the mid-eclipse time:

$$\text{JD}2448631.5 \pm 0.1 + N(3.4535 \pm 0.0005)$$

The folded data with the model superimposed is shown in figure 1. The mean X-7 count rate in the constant part of the model is found to be ≈ 13 counts ks^{-1} .

3.2 Evidence for a 0.31s pulsation

To search for periodicities at high frequencies, we split the PSPC and HRI data into 500s intervals of continuous data where X-7 is positively detected (i.e. we exclude the eclipse intervals) and calculated the summed Rayleigh power spectrum as described in the appendix. By doing so we lose about half of the available data to poor statistics. Smaller intervals would have resulted in less data being used because of the necessity to have at least 5 counts in each interval (see appendix A) while there are few continuous data intervals longer than 1000s. Choosing an interval length of 1000s instead of 500s did not substantially change the conclusions.

The resulting summed power spectrum is binned (reducing our frequency resolution) to increase signal-to-noise. Assuming a χ^2 distribution for the power (see appendix A), logarithmic bins in frequency showed no deviations from Poisson statistics such as red noise in our range of 10^{-3} –10 Hz (photons are time-tagged to a resolution of $\sim 10^{-3}$ s). However, the data showed a significant (99.9% confidence) power enhancement at 3.17 ± 0.08 Hz with linear binning, the error being the half-width of the peak in figure 2. The signal is washed out with logarithmic binning because of the corresponding poorer frequency resolution. Bin sizes of 70 to 120 independent Fourier spacings gave similar results.

As discussed in the appendix, we relied on 1000 simulated Poisson fluxes to fully assess the significance of this peak. The total number of counts n in each simulated flux is drawn from a Poisson distribution with the X-7 mean flux. Using the properties of Poisson fluxes, the n arrival times are uniformly drawn between 0 and the exposure time, sorted and then shifted to account for the observation time window. The simulated data is processed as with X-7. A Kolmogorov–Smirnov test comparing the power distribution of the X-7

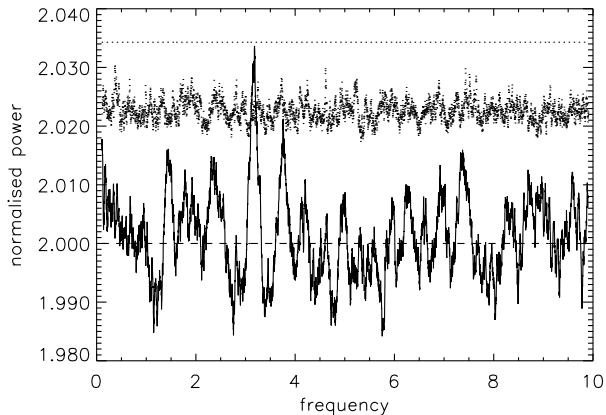


Figure 2. Fourier power spectrum for X-7. The power spectra of 500-s data intervals from the PSPC and HRI have been summed together. The total power spectrum was then smoothed by averaging the nearest 100 contiguous frequencies (there are 5000 independent frequencies in the non-averaged power spectrum). The dotted line is the theoretical 99.9% confidence level assuming a χ^2 statistic for the power distribution (the dashed line at $y=2$ being the expected average) and the dots represent the maximum power found at each frequency in the 1000 simulated fluxes (i.e. the calculated 99.9% confidence level see section 3.2).

spectrum with that calculated from the simulations showed no deviations, meaning the simulations adequately represented the flux from X-7. The maximum power at each frequency from the 1000 simulations gives an estimate of the 99.9% confidence level. As expected (see appendix), the peak in figure 2 is clearly above the maximum powers found in the simulations. This result is unchanged if Poisson fluxes are simulated with *exactly* the same number of counts as X-7 in each continuous interval (to account for the eclipses).

Though the feature seems broader than what would be expected from a simple sinusoidal pulse, it is not broad enough to qualify as a quasi-periodic oscillation (see e.g. van der Klis, 1989) and we therefore interpret it as an X-ray pulse. Knowing from the lightcurve the eclipse phase and orbital period, we tried correcting the photon times for their travel time across the system assuming a circular orbit. This did not lead to conclusive results. The Doppler effect and a non-zero pulse derivative are not enough to explain the observed peak width ~ 0.1 Hz. Assuming a ~ 50 light-second binary separation by analogy with SMC X-1 (see discussion), the Doppler shift is only of the order of 10^{-3} Hz. A frequency drift of the order of 0.1 Hz over ~ 5 years implies $\dot{\nu} \sim 10^{-10}$ Hz s^{-1} , at least an order of magnitude higher than what is observed in galactic X-ray pulsars.

Our data spans ~ 5 years, implying a folding frequency resolution of $\sim 10^{-9}$ Hz. As the count rate is not high enough to detect the pulsation within each observation we cannot fold the data and give a pulse shape with confidence. This is not in contradiction with the power spectrum analysis which does not include phase information (i.e. the distribution of observations in time). At this point it is not possible to check if the variability is coherent. Although pulsed emission seems a reasonable assumption, the power excess could arise from variability of a different nature (e.g. broadband variability increasing the chance of spurious detection).

4 DISCUSSION

4.1 The orbital lightcurve

Our well-sampled orbital lightcurve (figure 1) shows clearly that the X-7 eclipse ingress is gradual, but the egress is fast. This is compatible with the standard picture of an extended region of the disc which precedes the secondary in phase, analogous with features well-known in low-mass X-ray binaries (see e.g. White *et al* 1995). In high inclination systems this extended disc region (created by the impact of the mass transfer stream on the disc) will start to obscure the compact object before its eclipse by the secondary. We therefore believe that Roche-lobe overflow plays a significant role in X-7, even if it is a HMXB.

4.2 System parameters

As a 3.45-d eclipsing system with a 0.31-s pulse period, X-7 is very similar to the high mass X-ray binary SMC X-1 which has an orbital period of 3.89-d, a pulse period of 0.71-s and an X-ray luminosity of $5 \cdot 10^{38}$ erg s^{-1} (van Paradijs & McClintock 1995). The 10^{38} erg s^{-1} luminosity of X-7 is compatible with the Eddington luminosity of a neutron star accreting at $\sim 10^{-8} M_{\odot} \text{yr}^{-1}$. As is the case with SMC X-1, the companion is likely to be an O or B star, as suggested by the location of X-7's error box in the dense OB association HS13 (Humphreys & Sandage 1980). Roche lobe overflow is also significant in SMC X-1 (van Paradijs & McClintock 1995), and so we shall assume in our calculations that the mass-losing star in X-7 either fills or is close to filling its Roche lobe.

Under this assumption, we take $R_{\text{Roche}} = R_2$ to be the radius of the star, and adopt a binary inclination of 90° . We can now use our observed eclipse duration of 0.20 in phase to give $R_2/a = 0.59$, where a is the binary separation. Now the ratio of the Roche lobe radius to a is (for circular orbits) a function only of the mass ratio $q (=M_X/M_2)$ of the binary (Eggleton 1983), from which we derive $q = 0.085$. Combining this with Kepler's third law and an assumed compact object mass of $1.4 M_{\odot}$ (a canonical neutron star mass for our observed X-ray pulsar) gives $a = 25 R_{\odot}$, $M_2 = 16.4 M_{\odot}$ and $R_2 = 14.8 R_{\odot}$. This corresponds to an early-type star, and is significantly larger than a ZAMS star (which would have a radius of only $5.8 R_{\odot}$ for this mass). These parameters are consistent with a B0III star which has $M_V = -5.1$.

However, the inclination could be as low as 70° , for which our data would then give $q = 0.036$, $a = 32.9 R_{\odot}$, $M_2 = 39 M_{\odot}$ and $R_2 = 21 R_{\odot}$. Such a star is closer to a somewhat brighter ($M_V = -6.5$) O7I spectral type, and gives an indication of the uncertainties involved in this calculation. Interestingly, the brightest star in HS13 has $V = 18.8$ and, with a distance modulus of 24.65 (Humphreys & Sandage 1980), this corresponds to an absolute magnitude mid-way between the B0III and O7I spectral types.

5 CONCLUSION

We confirm M33 X-7 has an eclipse period of 3.45 days as Larson & Schulman (1997) had found using data from different satellites. Using a Fourier power spectrum method

adapted to low count rates, we also find evidence for a 0.31-s period, which identifies the compact object as a neutron star. From our best fit to the orbital lightcurve, we find the companion is an early type O or B star with $M \geq 15M_{\odot}$ and which is likely to be losing mass predominantly by Roche lobe overflow. The optical location of X-7 within a dense O-B association is consistent with the expected massive companion. When identified, the optical counterpart is likely to show ellipsoidal and/or heating variations (van Paradijs & McClintock 1995).

ACKNOWLEDGMENTS

We would like to thank D. Pelat, J.-L. Masnou, S. Bonazzola, M. van der Klis and the referee for helpful comments on this paper. We also acknowledge help from E. Schulman in obtaining all the archival observations of M33. We acknowledge support by the British-French joint research programme *Alliance*, by NASA grant NAG 5-1539 to the STScI and by the Academy of Finland. This research has made use of data obtained through the High Energy Astrophysics Science Archive Research Center Online Service, provided by the NASA-Goddard Space Flight Center.

REFERENCES

- van den Bergh S., 1991, *PASP*, 105, 609
 Brazier, K.T.S., 1994, *MNRAS*, 268, 709
 David L.P., Harnden F.R. Jr., Kearns K.E., Zombeck M.V., Feb. 1996, The *ROSAT* High Resolution Imager (HRI) Calibration Report, U.S. *ROSAT* Science Data Center/SAO
 Dubus G., Charles P.A., Long K.S., Hakala P.J., 1997, *ApJ*, 490, L47 (paper I)
 Eggleton P.P., 1983, *ApJ*, 268, 368
 Humphreys R.M., Sandage A., 1980, *ApJS*, 44, 319
 Larson D.T., Schulman E., 1997, *A.J.*, 113, 618
 Leahy D.A., et al., 1983, *ApJ*, 266, 160
 Long K.S., D’Odorico S., Charles P.A., Dopita M.A., 1981, *ApJ*, 246, L61
 Long K.S., Charles P.A., Blair W.P., Gordon S.M., 1996, *ApJ*, 466, 750
 Markert T.H., Rallis A.D., 1983, *ApJ*, 275, 571
 Peres G., Reale F., Collura A., Fabbiano G., 1989, *ApJ*, 336, 140
 Schulman E., Bregman J.N., 1995, *ApJ*, 441, 568
 Schulman E., Bregman J.N., Collura A., Reale F., Peres G., 1993, *ApJ*, 418, L67
 Schulman E., Bregman J.N., Collura A., Reale F., Peres G., 1994, *ApJ*, 426, L55
 Trinchieri G., Fabbiano G., Peres G., 1988, *ApJ*, 325, 531
 Trümper J., 1984, *Phys. Scripta*, T7, 209
 van der Klis M., 1989, in *Timing Neutron Stars*, ed. H. Ogelman & E.P.J. van den Heuvel, NATO ASI, Kluwer: Dordrecht, p27
 van Paradijs J., McClintock J.E., 1995, in *X-ray binaries*, ed. W.H.G. Lewin, J. van Paradijs, E.P.J. van den Heuvel, Cambridge University Press
 de Vaucouleurs G., Leach R.W., 181, *PASP*, 93, 190
 White N.E., Nagase F., Parmar, A., 1995, in *X-ray binaries*, ed. W.H.G. Lewin, J. van Paradijs, E.P.J. van den Heuvel, Cambridge University Press

APPENDIX A: TIME ANALYSIS AT HIGH FREQUENCIES

A1 Motivation

Searching for periodicities in our observations with the Lomb-Scargle periodogram proved impractical at high frequencies > 0.001 Hz (the timescale of an orbit). First, the periodogram only extends to the Nyquist frequency of the data which is inversely proportional to the bin size chosen for the time series. The flux from X-7 being rather weak, small bin sizes imply long time series of zeros with a few 1’s at the binned photon arrival times. This can be computationally problematic to handle. Second, the folding frequency resolution of $\sim 10^{-9}$ Hz for our dataset leads to an enormous number of frequencies to search above 0.001 Hz.

In a Fourier analysis, it is thus customary (e.g. van der Klis, 1989) to split long observations into S smaller continuous intervals of *equal length*, bin the photon arrival times on some multiple of the satellite clock and then sum the resulting renormalised (Leahy et al. 1983) Fast Fourier Transforms (FFT). With the Leahy renormalisation, the power density probability follows a χ_{2S}^2 law when the number of counts in each interval is sufficiently large. Splitting observations increases the signal-to-noise ratio as compared to a single interval power spectrum by a factor \sqrt{S} , though at the price of frequency resolution.

A2 Rayleigh power

Binning makes no sense with a small number of events so, instead of the Leahy power spectrum, we calculated a Rayleigh power spectrum for each interval :

$$\frac{n}{2} F_n(\nu) = \left(\sum_{k=1}^n \cos(2\pi\nu t_k) \right)^2 + \left(\sum_{k=1}^n \sin(2\pi\nu t_k) \right)^2$$

if n photons were recorded at times t_k in the interval $[0, T]$ and ν is one of the independent frequencies $\{1/T, 2/T, \dots\}$. The Rayleigh power is essentially the Fourier power of the photon arrival times modeled as diracs at t_k (infinitely small bin size). The only limits to the highest sampled frequency are the time-tagging resolution of the instrument or the computation time requirements. As above, the power density probability follows a χ_2^2 law when the number of counts in the interval is sufficiently large ($n \gtrsim 100$; see Brazier, 1994, and references therein).

However, the probability law is already quite close to a χ_2^2 when $n \gtrsim 5$ though the tail of the distributions statistically differ. In practice, simulations show that the probability to have a large value for $F_n(\nu)$ when $5 \lesssim n \lesssim 100$ is smaller than the corresponding probability for a χ_2^2 distribution i.e. the significance of a high peak value in the power spectrum will be under-estimated if it is calculated with a χ_2^2 distribution. If one assumes the χ_2^2 is still an adequate representation of the power probability law even with low n , then the techniques described by van der Klis (1989) for the Leahy renormalised power spectra can be similarly applied (summed intervals, frequency binning). If a signal is detected (the threshold will in effect be more stringent than if n is large), the actual significance has to be estimated through simulations (see section 3.2).